AIDS

DOI: 10.1097/QAD.0000000000000971

Co-delivery of HIV-1 entry inhibitor and NNRTI shuttled by nanoparticles: cocktail therapeutic strategy for antiviral therapy

Wen Li[1], Fei Yu[1], Qian Wang[1], Qianqian Qi[1,2], Shan Su[1], Lan Xie[3], Lu Lu[1]*, Shibo Jiang[1,2,4]*

[1]Key Laboratory of Medical Molecular Virology of Ministries of Education and Health, Basic Medical College and Shanghai Public Health Clinical Center, Fudan University, Shanghai, 200032, China; [2]Lindsley F. Kimball Research Institute, New York Blood Center, New York, New York 10065, USA; [3]Beijing Institute of Pharmacology & Toxicology, Beijing, 100850, China; [4]Shanghai Institute of Planned Parenthood Research, Shanghai, 200032, China.

* Correspondence to Shibo Jiang or Lu Lu, Basic Medical College, Fudan University, Shanghai 200032, China.

Tel: +86-021-54237673; Fax: +86-021-54237465; E-mails: shibojiang@fudan.edu.cn or lul@fudan.edu.cn

Abstract

Objectives: Traditionally, the antiviral efficacy of classic cocktail therapy is significantly limited by the distinct pharmacokinetic profiles of partner therapeutics that lead to inconsistent *in vivo* bio-distribution. Here we developed a new cocktail-like drug delivery vehicle using biodegradable polymeric nanoparticles (NP) encapsulating non-nucleoside reverse transcriptase inhibitor (NNRTI) DAAN-14f (14f), surface-conjugated with HIV-1 fusion inhibitor T1144, designated T1144-NP-DAAN-14f (T1144-NP-14f), and aiming to achieve enhanced cellular uptake, improved antiviral activity and prolonged blood circulation time.

Methods: T1144-NP-14f was prepared through the emulsion/solvent evaporation technique and a maleimide-thiol coupling reaction. Particle size and morphology were determined by dynamic light scattering detection and transmission electron microscopy. Anti-HIV-1 activity was assessed by HIV-1 Env-mediated cell-cell fusion and infection by laboratory-adapted, primary, and resistant HIV-1 isolates, respectively. The *in vitro* release of 14f was investigated using the equilibrium dialysis method, and the pharmacokinetic study of T1144-NP-14f was performed on Sprague-Dawley rats.

Results: T1144-NP-14f displayed a spherical shape under TEM observation and had a size of 117 ± 19 nm. T1144-NP-14f exhibited strongest antiviral activity against a broad spectrum of HIV-1 strains, including NNRTI-, T1144-, or T20-resistant isolates, respectively. Both *in vitro* release and *in vivo* pharmacokinetic profile showed that

T1144-NP-14f exhibited a sustained controlled release behavior.

Conclusions: Our results demonstrated that the combination of entry inhibitor with NNRTI encapsulated in nanoparticles (T1144-NP-14f) was highly effective in inhibiting HIV-1 infection. This new cocktail-like drug delivery platform could serve as an effective anti-HIV-1 regimen by taking advantage of the extrinsic and intrinsic antiviral activity of individual drugs.

Keywords:

HIV-1, nanoparticles, entry inhibitor, non-nucleoside reverse transcriptase inhibitor, combination antiretroviral therapy, drug delivery system

Introduction

In recent years, human immunodeficiency virus type 1 (HIV-1) has become one of the deadliest infectious diseases among adults. Globally, acquired immune deficiency syndrome (AIDS) induced by HIV infection has killed more than 25 million people (http://www.unaids.org). UNAIDS estimates about 33 million people living with HIV/AIDS worldwide, including approximately 4.5 million youths and 2.1 million adolescents. Although many infected individuals have access to highly active antiretroviral therapy (HAART), new drugs and drug delivery strategies that offer improvements in potency and activity against HIV, even against multidrug-resistant HIV-1 viruses, are urgently needed [1, 2].

To date, most approved HIV medicines belong to the class of reverse transcriptase inhibitors and protease inhibitors [3]. However, clinical application of these inhibitors has been largely limited by the short half-life after administration, rapid induction of drug resistance, and high cost [4]. For example, enfuvirtide (also known as T20), which was the first HIV fusion inhibitor approved by FDA, exhibited favorable anti-HIV efficacy by interfering with the target cell to block the fusion of viral and cellular membrane [1, 5]. However, the drawbacks, including short *in vivo* half-life (less than 3 h) and the emergence of T20-resistant strains, have significantly impeded the broad clinical application of T20 [6-9]. Furthermore, the therapeutic potency of T20 cannot be increasingly enhanced by the lack of the gp41 pocket-binding domain.

Drug delivery systems based on nanotechnology have offered approaches resulting in the development of a "diverse toolbox" for disease treatment [10]. A case in point is represented by therapeutic peptides or small-molecule drugs conjugated/incorporated into versatile nanoparticles that exhibit well-recognized advantages, including hydrophilic and hydrophobic multidrug co-incorporation, prolonged circulation time *in vivo*, decoration with functionalized ligands, and enhanced patient compliance [11, 12]. Among a myriad of successful applications, nanoparticles for anti-HIV treatment have emerged as an especially promising drug delivery platform in comparison to conventional drug delivery formulations as a consequence of decreased drug clearance rate at physiological condition and

controlled, site-specific drug release, thus reducing unwanted side effects [13, 14]. More importantly, nanoparticle drug delivery strategies can effectively circumvent the P-glycoprotein (Pgp) efflux process, which can significantly enhance intracellular drug concentration [15]. Our previous study showed that the reverse transcriptase inhibitor DAAN-15h, which was encapsulated in PEG-PLA NP, exhibited high antiviral activities in MT-2, M7, and TZM-b1 cells expressing CD4 receptor and CCR5 or CXCR4 co-receptor compared to DAAN-15h drug solution [16]. Therefore, the integration of anti-HIV drugs with nanoparticles can broaden drug delivery flexibility and the scope of drug design, allowing for promising applications in the anti-HIV treatment field.

Combination therapy holds considerable appeal in enhancing antiviral activity by achieving synergistic effects and has been validated as more effective than monotherapy [17-20]. However, the general administration of a "cocktails"-based combination therapy often suffers from distinct pharmacokinetic profiles of different therapeutics that lead to inconsistent *in vivo* bio-distribution and, hence, inefficient therapy [21-23]. To address this dilemma, a new cocktail-like drug delivery vehicle using biodegradable nanoparticles was developed in this study. Specifically, we took advantage of functional maleimide groups on PEG chains and employed biocompatible Mal-PEG-PLA to engineer the nanoparticles with encapsulated NNRTI-DAAN-14f (14f) and surface-conjugated T1144 peptide, a third-generation HIV fusion inhibitor with enhanced antiviral activity (Fig. 1a). As an extrinsic (i.e.,

extracellular) combinatorial component, peptide T1144 would be expected to bind to the exposed grooves on the pre-fusion intermediate (PFI) and inhibit the fusion of virus with the target cell membrane [24], whereas the intrinsic (i.e., intracellular) combinatorial component, encapsulated NNRTI 14f, would be expected to internalize, diffuse and interact with a highly hydrophobic cavity in reverse transcriptase in a noncompetitive manner and allosterically block the chemical step of DNA synthesis (Fig. 1b) [25, 26]. As such, the integration of T1144 and 14f in a single nanoparticle offers a combinatorial antiviral effect against a broad spectrum of HIV-1 strains, including multidrug-resistant mutants. Moreover, the new cocktail-like drug delivery vehicle T1144-NP-DAAN-14f (T1144-NP-14f) holds other advantages, including enhanced intracellular uptake, sustained controlled release behavior, and prolonged blood circulation time *in vivo*. We believe this new strategy for anti-HIV treatment holds promise in overcoming the limitations and drawbacks of conventional single anti-HIV drug delivery at both research and clinical levels.

Materials and Methods

Animals and Materials

Methoxy-poly (ethylene glycol) 3000-poly (lactic acid) 34000 (MePEG-PLA) and maleimide-poly (ethylene glycol) 3400-poly (lactic acid) (Mal-PEG-PLA) were obtained from the University of Electronic Science and Technology of China (UESTC). Peptides T1144, N36, and C34 were synthesized by a standard solid-phase

FMOC method at GL Biochem Ltd. (Shanghai, China). The peptides were purified to homogeneity (> 99% purity) by HPLC and verified by mass spectrometry. The cells (MT-2, M7, and TZM-b1), the laboratory-adapted HIV-1 strains IIIB and Bal, and the primary HIV-1 isolates, including the NNRTI-resistant HIV-1 strains, the T1144-resisitant HIV-1 strains, and the T20-resistant strains, were obtained from the NIH AIDS Research and Reference Reagent Program. The small molecule NNRTI 14f was synthesized as previously described [27].

Six- to eight-week-old male Sprague-Dawley (SD) rats were used in the study. The animal studies were carried out in strict accordance with the recommendations in the Guide for the Care and Use of Laboratory Animals of Fudan University.

Preparation of T1144-NP-14f

Nanoparticles (NP) loaded with 14f were prepared through the emulsion/solvent evaporation technique according to the procedure described previously [28]. First, 22.5 mg MePEG-PLA, 2.5 mg Mal-PEG-PLA and 14f (100 μg) were dissolved in 1 ml dichloromethane, after which 2 ml of 1% sodium cholate aqueous solution were added and emulsified by sonication (240 w, 30 s) with a sonicator in ice bath. After sonication, the emulsion was added into 8 ml of 0.5% sodium cholate aqueous solution under rapid stirring for 5 min. The emulsion was subsequently subjected to a rotary evaporator to remove the dichloromethane, followed by centrifugation at 15000 rpm for 1 h. The supernatant was discarded, and the nanoparticles (NP-14f) were resuspended in distilled water and stored at 4 ^{o}C for

further use.

T1144-functionalized nanoparticles (T1144-NP-14f) were prepared *via* a maleimide-thiol coupling reaction at room temperature for 8h as described previously [29]. T1144-NPs were prepared as described above without adding 14f, and blank NPs were prepared without adding 14f and conjugating with T1144. Coumarin-6-labled NPs were prepared with the same procedure, except that coumarin-6 was added to the mixture instead of 14f.

Characterization of the nanoparticles

Particle size and zeta potential of blank NP, NP-14f, and T1144-NP-14f were determined by dynamic light scattering (DLS) detection (Wyatt Technology, Santa Barbara, CA, USA).

Morphological examination of blank NP, NP-14f, and T1144-NP-14f was performed by transmission electron microscopy (TEM) (H-600, Hitachi, Japan), following negative staining with phosphotungstate solution.

Detection of inhibition of 6-HB formation by ELISA

The sandwich ELISA for testing inhibitory activity of a drug against gp41 six-helix bundle (6-HB) formation was described previously [30, 31]. Briefly, tested drugs (NP, 14f, T1144, NP-14f, T1144-NP, and T1144-NP-14f) at graded concentration were mixed with N36 peptide (2 μM) and incubated at 37 ^{o}C for 30 min, followed by addition of C34 (1 μM) and again incubated at 37 ^{o}C for 30 min. Then the mixture was added to a 96-well polystyrene plate, which was precoated with

a 6-HB-specific monoclonal antibody (mAb), NY-364 IgG (2 μg/ml in 0.1 M Tris, pH 8.8), and then incubated at 37 ^{o}C for 1 h and washed with PBST (PBS + 0.05% Tween-20). Next, the mAb NC-1, horseradish peroxidase-labeled rabbit-anti-mouse IgG and the substrate 3, 3', 5, 5'-tetramethylbenzidine (TMB) were added sequentially. Absorbance at 450 nm was detected using an ELISA reader (Tecan, USA).

Measurement of the inhibitory activities of T1144-NP-14f on infection by HIV-1 strains with different subtype and tropism

The inhibitory activities of T1144-NP-14f on infection by HIV-1 IIIB virus (subtype B, X4) were tested in MT-2 cells by p24 assay as previously described [32-34]. In brief, 1×10^4 MT-2 cells were infected with HIV-1 virus at 100 TCID50 (50% tissue culture infective dose) overnight in 200 μl RPMI 1640 medium containing 10% FBS in the presence or absence of T1144-NP-14f at graded concentration. The supernatant was then replaced with fresh medium, and on the fourth day post-infection, 100 μl of culture supernatant were collected from each well and mixed with equal volume of 5% Triton X-100, followed by detection of the p24 antigen by ELISA, as previously described [35]. The inhibition of infection by NNRTI-resistant strains, T1144-resistant strains, and T20-resistant strains was detected in MT-2 cells by p24 assay as described above [32-34].

In order to test the antiviral activities of T1144-NP-14f in HIV-1 Bal (subtype B, R5) and primary HIV-1 isolates, 50μl T1144-NP-14f at graded concentrations were

incubated with HIV-1 virus at 100 TCID50 for 30 min, followed by the addition of 100 μl M7 cells (1×10^5 cells/ml). The culture supernatant was changed with fresh RPMI 1640 medium containing 10% FBS overnight. On the seventh day post-infection, 100 μl culture supernatant were collected from each well and mixed with equal volume of 5% Triton X-100, followed by detection of the p24 antigen. The IC50 values were calculated with Calcusyn software, kindly provided by Dr. T. C. Chou at Sloan-Kettering Cancer Center (New York, NY) [36, 37].

***In vivo* pharmacokinetic studies of 14f solution, NP-14f, and T1144-NP-14f**

In vivo pharmacokinetics of 14f solution, NP-14f, and T1144-NP-14f was investigated using SD rats (200 ± 20 g), which were obtained from the Experimental Animal Center of Fudan University, housed at 25 ± 1 °C with access to food and water ad libitum, and handled in accordance with the Guide for the Care and Use of Laboratory Animals of Fudan University. Nine SD rats were randomly divided into three groups (n = 3). The rats were then injected with 14f solution, NP-14f, and T1144-NP-14f suspended in sterile saline solution at the dose of 5 mg 14f/kg through the tail vein. At predetermined time points (0.083, 0.25, 0.5, 1, 2, 4, 6, 8, 12, 16, 24, and 48 h), blood samples were collected from the carotid vein and centrifuged at 800 g for 10 min with the supernatant stored at -20 ^{o}C until analysis.

Blood concentration of 14f was determined by reverse-phase high performance liquid chromatography coupled with tandem mass spectrometry (LC-MS/MS) detection. To prepare samples for analysis, 120 μl methanol containing 50

ng/ml warfarin (internal standard) were added into 30 μl plasma to precipitate the protein. The mixture was vortexed and subsequently centrifuged at 12000 rpm for 10 min with the supernatant mixed with an equal volume of distilled water and subjected to liquid chromatography-tandem mass spectrometry (LC-MS/MS) analysis. The pharmacokinetics data analysis was performed by means of a model-independent method. All concentration data were dose-normalized and plotted as plasma drug concentration-time curves. Drug and Statistics software for Windows (DAS ver. 2.1.1) was utilized to calculate the pharmacokinetics parameters.

Results

Characterization and biophysical determination of T1144-NP-14f

The nanoparticles were prepared *via* emulsion/solvent evaporation. T1144-NP and T1144-NP-14f were obtained *via* a maleimide-thiol coupling reaction. Particle sizes, polydispersity indexes (PDI), and zeta potentials of blank NP, NP-14f, and T1144-NP-14f were determined by dynamic light scattering detection. As shown in Figure 2a, b, and c, the sizes of NP, NP-14f and T1144-NP-14f were 92.8 ± 5.3 nm, 97.0 ± 15.6 nm, and 117.0 ± 18.9 nm, respectively. The encapsulation of NNRTI 14f did not significantly increase the particle size of NP. The increased particle size after T1144 conjugation suggested the existence of T1144 peptide on the surface of NP-14f. The zeta potentials of NP, NP-14f, and T1144-NP-14f were –28.6 ± 4.7 mV, –24.3 ± 3.36 mV, and –20.1 ± 5.2 mV, respectively (Table S1, http://links.lww.com/QAD/A838).

Representative TEM images illustrated that blank NP, NP-14f, and T1144-NP-14f exhibited a similar spherical shape (Fig. 2d, e, and f). The T1144-NP-couamrin-6 assembly was observed by colocalization of the fluorescence signals of coumarin-6 (green) in the nanoparticles and Rhodamine (red) in the Rhodamine-labled T1144 peptide (Fig. 2g). The LC of NP-14f and T1144-NP-14f, as detected by HPLC, was 1.53 ± 0.03% and 1.37 ± 0.06%, with EE of 48.3 ± 2.3% and 47.6 ± 1.6%, respectively.

Coumarin-6 was used as the fluorescent probe to study the performance of different 14f formulations in MT-2 cells and M7 cells. As shown in Figure 3a and 3b, the cellular internalization of T1144-NP-coumarin-6 and NP-coumarin-6 in MT-2 cells and M7 cells was higher than dissociative coumarin-6 at coumarin-6 concentrations ranging from 25 ng/ml to 600 ng/ml at 37 ^{o}C and 4 ^{o}C, respectively. In addition, the uptake by MT-2 cells and M7 cells were temperature-dependent which was illustrated by the higher fluorescence signal at 37 ^{o}C when compared to 4 ^{o}C. Time-dependent uptake profiles could be observed with the 15 to 30-fold higher cellular uptake of T1144-NP-coumarin-6 than coumarin-6 solution by MT-2 and M7 cells at the incubation time ranging from 0.5 h to 8 h (Figure 3c and 3d). Therefore, the cellular internalization of T1144-NP-coumarin-6 occurred in concentration-, temperature-, and time-dependent manner.

The cellular uptake mechanism of T1144-NP-coumarin-6 and NP-coumarin-6 in MT-2 and M7 lymphocytes was determined by using various endocytosis inhibitors.

Inhibition experiments showed that the cellular uptake of T1144-NP-coumarin-6 and NP-coumarin-6 were inhibited by energy-depletion agent-NaN3 + deoxyglucose, lipid raft inhibitor-MCD, and lysosome inhibitor-monension (Figure S1, http://links.lww.com/QAD/A838).

The intracellular delivery of NP-coumarin-6 and T1144-NP-coumarin-6 in TZM-b1 cells was also investigated using confocal laser scanning microscopy (CLSM). NP-coumarin-6 and T1144-NP-coumarin-6 were internalized by cells *via* lipid draft-mediated lysosome pathway. As shown in Figure S2, most of the endocytosed NPs were found in lysosome and late endosome judged by the colocalization of green fluorescence (NPs) and red fluorescence (Rhodamine-labeled lysosome and late endosome). The observation result was consistent well with the interlization inhibition experiments.

The formation of 6-HB fusion core is a critical step during HIV-1 fusion with the target cell. T1144 was able to bind to viral gp41 N-trimer NHR to block 6-HB fusion core formation [38]. Here a sandwich ELISA was used to determine whether T1144-NP-14f possessed inhibitory activity on gp41 6-HB formation. As shown in Figure 4a, T1144-NP-14f inhibited 6-HB formation in a dose-dependent manner similar to that of free T1144 peptide with IC_{50} of 4.77μM. These results indicated that T1144-NP-14f could interact with gp41 NHR and block 6-HB core formation between viral gp41 NHR and CHR. In the HIV-1 Env-mediated cell-cell fusion assay (Fig. 4b), T1144-NP-14f, T1144-NP, and T1144 peptide could inhibit the cell-cell fusion between

H9/IIIB and MT-2 cells with IC_{50}s of 9.78 nM, 8.86 nM, and 8.38 nM, respectively.

Increased antiviral activities of T1144-NP-14f against laboratory-adapted, primary HIV-1 isolates, and HIV-1-resistant strains with different subtypes and tropism

As shown in Figure 4c and 4d, T1144-NP-14f showed enhanced antiviral activity against laboratory-adapted HIV-1 strains IIIB (X4) and Bal (R5) compared with 14f solution, T1144, T1144-NP, and NP-14f, respectively. The IC50 values of T1144-NP-14f against HIV-1 IIIB and Bal were 0.24 nM and 0.13 nM, which are 20.95- and 36.03-fold higher, respectively, than that of 14f solution against HIV-1 infection, as well as 25.12- and 40.13-fold higher, respectively, than that of T1144 peptide. The potential cooperative effects of T1144-NP-14f against HIV-1 IIIB and Bal strains were compared with T1144 combined with 14f solution. Results showed that T1144-NP-14f exhibited stronger synergistic effect against HIV-1 IIIB and Bal strains (CI: 0.05 ~ 0.08) than that demonstrated by T1144 peptide combined with 14f solution (CI: 0.13 ~ 0.25). Additionally, T1144-NP-14f displayed very strong synergism against 7 representative primary isolates of HIV-1, covering clades A, B, C, D, F, O and A/E subtypes X4, R5 or X4/R5 (CI: 0.03 ~ 0.1), with dose reductions of 19.7 ~ 69.1-fold for T1144 peptide and 17.9 ~ 67.6-fold for 14f solution based on the IC_{50} values (Table S2 and Table S3, http://links.lww.com/QAD/A838). Notably, T1144-NP-14f showed higher potency than 14f against HIV-1 NNRTI-resistant

strains, including A17, RTMDR1, and Nevirapine-resistant strain with dose reduction of 5.71 ~ 23.99-fold. Furthermore, T1144-NP-14f possessed potent inhibitory activities against T1144- and T20-resistant strains with dose reduction of 7.56- ~ 132.54-fold for T1144 and 6.2- ~ 82.82-fold for 14f, respectively (Table S4, http://links.lww.com/QAD/A838). These results suggest that T1144-NP-14f possesses much more potent antiviral activities against a broad spectrum of HIV-1 strains, which is promising for further development as an anti-HIV therapeutic drug.

Sustained release of 14f in both *in vitro* and *in vivo* pharmacokinetic studies

The *in vitro* release experiment showed that NP-14f and T1144-NP-14f presented almost the same release behavior (Fig. 5a). Biphasic drug release was observed for all nanoparticles. In the first 6 h, a burst release was achieved, while twenty-four hours later, the release rate slowed down. At the end of 96 h, the cumulative release of 14f from NP-14f was 78.25 ± 4.32% and 76.52 ± 3.68% from T1144-NP-14f. In contrast, more than 90% 14f was released from 14f solution within 6 h.

After intravenous administration of 14f solution, NP-14f, and T1144-NP-14f at the dose of 5 mg/kg, blood samples were collected and analyzed. Plasma 14f concentration-time profiles were shown in Figure 5b. The 14f solution exhibited fast blood clearance, short half-life and low AUC_{0-t} from systemic circulation. In contrast, much higher concentration and longer circulation time were achieved after encapsulation of 14f in nanoparticles. As shown in Figure 5b, 24 h post-injection, the

concentration of 14f solution was under the limit of detection, while NP-14f and T1144-NP-14f showed much higher concentration at all time points. NP-14f showed prolonged elimination half-life ($t_{1/2}$ 9.13 h), decreased clearance rate (CL 0.078 L/h), and extended $AUC_{0\text{-}24h}$ (63041.97 μg/L/h). Additionally, T1144-NP-14f exhibited elimination half-life of 9.08 h, clearance rate of 0.095 L/h, and $AUC_{0\text{-}24h}$ of 52536.01 μg/L/h *in vivo* (Table S5, http://links.lww.com/QAD/A838). No significant difference was found between NP-14f and T1144-NP-14f, indicating that the combination of T1144 peptide and NP-14f did not change the circulation behavior of nanoparticles.

Discussion

Nanotechnology has allowed versatile drug delivery platforms with high drug drug-loading capacity, as well as enhanced bioavailability and biocompatibility [39]. In this study, a new cocktail-like nanoparticle drug delivery system was developed by conjugating an HIV-1 entry inhibitor, T1144 peptide, on the surface of 14f-loaded NPs. This strategy addressed the current limitations for HIV-1 treatment, such as insufficient cellular internalization of drugs and short half-life *in vivo*. By combining the extracellular antiviral effect of T1144 peptide on the cell surface and the intracellular antiviral activity of 14f after internalization, we believe the new cocktail-like T1144-NP-14f drug delivery system could serve as an optimized therapeutic strategy to combat HIV-1 infection.

As shown in Figure 1, T1144 and 14f have different active destinations and, hence, the potential to block HIV-1 infection at different stages of the HIV-1 life cycle. T1144, as an entry inhibitor, could interact with gp41 NHRs and form 6-HB with N peptide (N36) to inhibit HIV-1 gp41-mediated virus-cell fusion, while the NNRTI-14f could interact with a highly hydrophobic cavity in reverse transcriptase (RT) in a noncompetitive manner to block the chemical step of DNA synthesis and, subsequently, block viral replication. Targeting multiple steps during the process of HIV-1 infection can reduce the development of new resistant viral strains [40, 41].

T1144-NP-14f nanoparticles were obtained through an emulsion/evaporation method with diameters of approximately 100 nm and an average narrow distribution [42, 43]. The cellular uptake and membrane transport mechanism of T1144-NP-14f showed significantly higher cellular internalization of T1144-NP-coumarin-6 and NP-coumarin-6 when compared with coumarin-6 solution (Fig. 3), indicating that the NP carrier could enhance the endocytosis of drug and T1144 peptide, but without affecting interaction between functionalized nanoparticles and MT-2 or M7 cells. Successful intracellular drug delivery is a key step to improve the efficiency of a nanoparticle-base therapeutic. To figure out the endocytosis pathway, we incubated MT-2 or M7 cells with several different inhibitors to reveal the endocytosis mechanism of T1144-NP-coumarin-6. The internalization of both NP-coumarin-6 and T1144-NP-coumarin-6 was significantly inhibited by NaN_3 + deoxyglucose, M-β-CD, and monensin, suggesting that the endocytosis of both NP-coumarin-6 and T1144-NP-

coumarin-6 was lipid raft-mediated and energy-dependent with lysosome-enabled transport [44-46]. Furthermore, confocal images showed the extensive distribution of NP after endocytosis at cytoplasm, which was the active destination of NNRTIs, as evidenced by the separated fluorescence of coumarin-6 and DAPI (Fig. S2, http://links.lww.com/QAD/A838). More importantly, the separated fluorescence of nanoparticle and lysosome indicated the efficient endosome escape, which was beneficial for intracellular functional drugs since the drugs entrapped in the endosome would be degraded. Taken together, the enhanced cellular uptake and efficient endosome escape ensured the sufficient intracellular drug concentrations, which built foundation for improved efficacy of NNRTIs.

The enhanced endocytosis of T1144-NP-14f by the nanoparticle drug carrier resulted in a significant increase of anti-HIV-1 potency. The inhibitory activity of T1144-NP-14f against infection of HIV-1 IIIB and Bal was 25.12- and 40.13-fold higher than that of T1144 peptide, respectively, and 20.95- and 36.03-fold higher than that of 14f solution (Fig. 4c and 4d). One possible mechanism underlying this increased antiviral activity could be attributed to the interaction between T1144 peptide and the gp41 NHR-trimer to block 6-HB formation, thus avoiding viral entry and subsequent infection of the target cells. On the other hand, 14f played a decisive role in reverse transcriptase inhibition, as evidenced by ELISA (Fig. 4a) and cell-cell fusion (Fig. 4b) examination.

The *In vitro* cytotoxicity experiment showed that 14f solution and NPs exhibited no

significant cytotoxicity to cells at the concentration of 14f or T1144 as high as 4000 nM (Fig. S3, http://links.lww.com/QAD/A838). These data indicated that enhanced internalization of T1144-NP-14f in MT-2 and M7 cells did not cause cytotoxicity, suggesting that PEG-PLA-based nanomaterials can be considered as safe polymer drug carriers for human use.

In vitro release of 14f was evaluated in PBS (pH 7.4) that showed an apparent biphasic release pattern for T1144-NP-14f and NP-14f. The release of 14f from T1144-NP-14f was significantly slower than that of 14f solution. The initial faster burst release was believed to derive from the agents that located at the outer layer of the particles, while the later and slower release appeared to result from agents affected by erosion or degradation of the matrix [47]. The pharmacokinetics profile of the T1144-NP-14f, NP-14f, and 14f formulations was studied on SD rats after intravenous administration. The 14f formulation exhibited quicker blood clearance, shorter half-life and lower AUC_{0-t} from systemic circulation, while T1144-NP-14f and NP-14f showed significantly prolonged elimination half-life, decreased clearance rate, and extended AUC_{0-24h}, suggesting that the nanocarrier was effective in facilitating the circulation of 14f molecules and that T1144 peptide did not change the circulation behavior of T1144-NP-14f. We concluded from these findings that the PEG polymer coating on the surface of NPs could improve the *in vivo* pharmacokinetics profile of T1144-NP-14f.

The emergence of nanotechnology has made a significant impact on the

development of clinical therapeutics, particularly providing an unparalleled opportunity for development of anti-HIV drugs. The application of nanotechnology offers the superiority of using anti-HIV drugs at lower dose, reduced systemic toxicity and enhanced therapeutic efficacy. However, translation of nanotechnology-based anti-HIV therapy into the clinics remains challenging. Significant efforts are needed to promote the translation process, including: 1) selection of absolutely biocompatible and biodegradable composition of nanoparticles; 2) carefully and rationally tailoring size and physicochemical property of the nanoparticles; and 3) providing desirable control over the drug biodistribution and pharmacokinetics to improve efficacy and reduce toxicity of nanoparticle-based anti-HIV therapeutics.

In conclusion, we employed biodegradable organic nanoparticles, PEG-PLA-NP, for encapsulation of anti-HIV-1 drug 14f and conjugation of T1144, a third-generation HIV-1 entry inhibitor, on the surface of nanoparticles. Our results demonstrated that the combination of entry inhibitor with reverse transcriptase inhibitor was highly effective in inhibiting R5-HIV-1 and X4-HIV-1, primary HIV-1 isolates, NNRTI-resistant HIV-1 strains, and T1144-resistant HIV-1 strains. Additionally, T1144-NP-14f exhibited enhanced intracellular uptake, sustained controlled release behavior and prolonged blood circulation time. The results indicated that the new cocktail-like nanoparticle drug delivery platform could serve as an effective anti-HIV-1 regimen by taking advantage of extrinsic and intrinsic antiviral activity of the partner drugs.

Acknowledgements

We are grateful to Dr. Jun Chen, School of Pharmacy, Fudan University, for providing help in liquid chromatography-tandem mass spectrometry (LC-MS/MS) analysis. We greatly appreciate the exchange program fund for doctoral students under the office for Graduate Medical Education, Fudan University, for supporting Wen Li's foreign research and living expenses. This work was supported by grants from the National Megaprojects of China for Major Infectious Diseases (2013ZX10001-006 and 2012ZX10001-007-008) to S.J., the National Science Fund of China (81361120378 to S.J. and 81373456 to L.L.), and the National 863 Program of China (2015AA020930 to L.L.).

W.L., F.Y., Q.W., Q.Q., and S.S. performed the experiments. L.X. provided the NNRTI. W.L. L.L., and S.J. proposed the project, analyzed the data, wrote the manuscript.

Conflicts of interest

There are no conflicts of interest.

Reference

1. Aberg JA, Gallant JE, Ghanem KG, Emmanuel P, Zingman BS, Horberg MA, *et al.* Primary care guidelines for the management of persons infected with HIV: 2013 update by the HIV Medicine Association of the Infectious Diseases Society of America. *Clin Infect Dis* 2014; **58(1)**:1-10.

2. Lalezari JP, Henry K, O'Hearn M, Montaner JS, Piliero PJ, Trottier B, *et al.* Enfuvirtide, an HIV-1 fusion inhibitor, for drug-resistant HIV infection in north and south America. *N Engl J Med* 2003; **348(22)**:2175-2185.

3. Pretorius E, Klinker H, Rosenkranz B. The role of therapeutic drug monitoring in the management of patients with human immunodeficiency virus infection. *Ther Drug Monit* 2011; **33(3)**:265-274.

4. Fellay J, Boubaker K, Ledergerber B, Bernasconi E, Furrer H, Battegay M, *et al.* Prevalence of adverse events associated with potent antiretroviral treatment: Swiss HIV Cohort Study. *Lancet* 2001; **358(9290)**:1322-1327.

5. Wainberg MA. AIDS: Drugs that prevent HIV infection. *Nature* 2011; **469(7330)**:306-307.

6. Liu S, Jing W, Cheung B, Lu H, Sun J, Yan X, *et al.* HIV gp41 C-terminal heptad repeat contains multifunctional domains: relation to mechanisms of action of anti-HIV peptides. *J Biol Chem* 2007; **282(13)**:9612-9620.

7. Poveda E, Briz V, Soriano V. Enfuvirtide, the first fusion inhibitor to treat HIV infection. *AIDS Rev* 2005; **7(3)**:139-147.

8. Rimsky LT, Shugars DC, Matthews TJ. Determinants of human immunodeficiency virus type 1 resistance to gp41-derived inhibitory peptides. *J Virol* 1998; **72**:986-993.

9. Wild CT, Shugars DC, Greenwell TK, McDanal CB, Matthews TJ. Peptides corresponding to a predictive alpha-helical domain of human immunodeficiency virus type 1 gp41 are potent inhibitors of virus infection. *Proc Natl Acad Sci USA* 1994; **91(□ı)**:9770-9774.

10. Farokhzad OC, Langer R. Impact of nanotechnology on drug delivery. *ACS Nano* 2009; **3(1)**:16-20.

11. Farokhzad OC, Langer R. Nanomedicine: developing smarter therapeutic and diagnostic modalities. *Adv Drug Deliv Rev* 2006; **58(14)**:1456-1459.

12. Hu Q, Katti PS, Gu Z. Enzyme-responsive nanomaterials for controlled drug

delivery. *Nanoscale* 2014; **6(21)**:12273-12286.

13. Mamo T, Moseman EA, Kolishetti N, Salvador-Morales C, Shi J, Kuritzkes DR, *et al.* Emerging nanotechnology approaches for HIV/AIDS treatment and prevention. *Nanomedicine (Lond)* 2010; **5(2)**:269-285.

14. Das NJ, Amiji MM, Bahia MF, Sarmento B. Nanotechnology-based systems for the treatment and prevention of HIV/AIDS. *Adv Drug Deliv Rev* 2010; **62(4-5)**:458-477.

15. Chavanpatil MD, Khdair A, Gerard B, Bachmeier C, Miller DW, Shekhar MP, *et al.* Surfactant-polymer nanoparticles overcome P-glycoprotein-mediated drug efflux. *Mol Pharm* 2007; **4(5)**:730-738.

16. Li W, Wang Q, Li Y, Yu F, Liu Q, Qin B, *et al.* A nanoparticle-encapsulated non-nucleoside reverse-transcriptase inhibitor with enhanced anti-HIV-1 activity and prolonged circulation time in plasma. *Curr Pharm Des* 2015; **21(7)**:925-935.

17. Cooper CL, van Heeswijk RP, Gallicano K, Cameron DW. A review of low-dose ritonavir in protease inhibitor combination therapy. *Clin Infect Dis* 2003; **36(12)**:1585-1592.

18. Gortmaker SL, Hughes M, Cervia J, Brady M, Johnson GM, Seage GR, III, *et al.* Effect of combination therapy including protease inhibitors on mortality among children and adolescents infected with HIV-1. *N Engl J Med* 2001; **345(21)**:1522-1528.

19. Xu W, Wang Q, Yu F, Lu L, Jiang S. Synergistic effect resulting from combinations of a bifunctional HIV-1 antagonist with antiretroviral drugs. *J Acquir Immune Defic Syndr* 2014; **67(1)**:1-6.

20. Wang Q, Bi W, Zhu X, Li H, Qi Q, Yu F, *et al.* Nonneutralizing Antibodies Induced by the HIV-1 gp41 NHR Domain Gain Neutralizing Activity in the Presence of the HIV Fusion Inhibitor Enfuvirtide: a Potential Therapeutic Vaccine Strategy. *J Virol* 2015; **89(13)**:6960-6964.

21. Lehar J, Krueger AS, Avery W, Heilbut AM, Johansen LM, Price ER, *et al.* Synergistic drug combinations tend to improve therapeutically relevant selectivity. *Nat Biotechnol* 2009; **27(7)**:659-666.

22. Hu CM, Aryal S, Zhang L. Nanoparticle-assisted combination therapies for effective cancer treatment. *Ther Deliv* 2010; **1(2)**:323-334.

23. Van Heeswijk RP, Veldkamp A, Mulder JW, Meenhorst PL, Lange JM,

Beijnen JH, *et al.* Combination of protease inhibitors for the treatment of HIV-1-infected patients: a review of pharmacokinetics and clinical experience. *Antivir Ther* 2001; **6(4)**:201-229.

24. Dwyer JJ, Wilson KL, Davison DK, Freel SA, Seedorff JE, Wring SA, *et al.* Design of helical, oligomeric HIV-1 fusion inhibitor peptides with potent activity against enfuvirtide-resistant virus. *Proc Natl Acad Sci USA* 2007; **104(31)**:12772-12777.

25. Fulco PP, McNicholl IR. Etravirine and rilpivirine: nonnucleoside reverse transcriptase inhibitors with activity against human immunodeficiency virus type 1 strains resistant to previous nonnucleoside agents. *Pharmacotherapy* 2009; **29(3)**:281-294.

26. Johnson BC, Pauly GT, Rai G, Patel D, Bauman JD, Baker HL, *et al.* A comparison of the ability of rilpivirine (TMC278) and selected analogues to inhibit clinically relevant HIV-1 reverse transcriptase mutants. *Retrovirology* 2012; **9**:99.

27. Sun LQ, Zhu L, Qian K, Qin B, Huang L, Chen CH, *et al.* Design, synthesis, and preclinical evaluations of novel 4-substituted 1,5-diarylanilines as potent HIV-1 non-nucleoside reverse transcriptase inhibitor (NNRTI) drug candidates. *J Med Chem* 2012; **55(16)**:7219-7229.

28. Hu Q, Gu G, Liu Z, Jiang M, Kang T, Miao D, *et al.* F3 peptide-functionalized PEG-PLA nanoparticles co-administrated with tLyp-1 peptide for anti-glioma drug delivery. *Biomaterials* 2013; **34(4)**:1135-1145.

29. Hu Q, Gao X, Gu G, Kang T, Tu Y, Liu Z, *et al.* Glioma therapy using tumor homing and penetrating peptide-functionalized PEG-PLA nanoparticles loaded with paclitaxel. *Biomaterials* 2013; **34(22)**:5640-5650.

30. Jiang S, Lin K, Zhang L, Debnath AK. A screening assay for antiviral compounds targeted to the HIV-1 gp41 core structure using a conformation-specific monoclonal antibody. *J Virol Methods* 1999; **80(1)**:85-96.

31. Zhu X, Zhu Y, Ye S, Wang Q, Xu W, Su S, *et al.* Improved Pharmacological and Structural Properties of HIV Fusion Inhibitor AP3 over Enfuvirtide: Highlighting Advantages of Artificial Peptide Strategy. *Sci Rep* 2015; **5**:13028.

32. Lu L, Pan C, Li Y, Lu H, He W, Jiang S. A bivalent recombinant protein inactivates HIV-1 by targeting the gp41 prehairpin fusion intermediate induced by CD4 D1D2 domains. *Retrovirology* 2012; **9**:104.

33. Tong P, Lu Z, Chen X, Wang Q, Yu F, Zou P, *et al.* An engineered HIV-1 gp41

trimeric coiled coil with increased stability and anti-HIV-1 activity: implication for developing anti-HIV microbicides. *J Antimicrob Chemother* 2013; **68(11)**:2533-2544.

34. Yu F, Lu L, Liu Q, Yu X, Wang L, He E, *et al.* ADS-J1 inhibits HIV-1 infection and membrane fusion by targeting the highly conserved pocket in the gp41 NHR-trimer. *Biochim Biophys Acta* 2014; **1838(5)**:1296-1305.

35. Lu H, Zhao Q, Wallace G, Liu S, He Y, Shattock R, *et al.* Cellulose acetate 1,2-benzenedicarboxylate inhibits infection by cell-free and cell-associated primary HIV-1 isolates. *AIDS Res Hum Retroviruses* 2006; **22(5)**:411-418.

36. Chou TC, Hayball MP. *CalcuSyn: Windows software for dose effect analysis*. Ferguson, MO 63135, USA: BIOSOFT; 1991.

37. Chou TC. Theoretical basis, experimental design, and computerized simulation of synergism and antagonism in drug combination studies. *Pharmacol Rev* 2006; **58(3)**:621-681.

38. Liu S, Lu H, Xu Y, Wu S, Jiang S. Different from the HIV fusion inhibitor C34, the anti-HIV drug Fuzeon (T-20) inhibits HIV-1 entry by targeting multiple sites in gp41 and gp120. *J Biol Chem* 2005; **280(12)**:11259-11273.

39. Shi J, Votruba AR, Farokhzad OC, Langer R. Nanotechnology in drug delivery and tissue engineering: from discovery to applications. *Nano Lett* 2010; **10(9)**:3223-3230.

40. Pirrone V, Thakkar N, Jacobson JM, Wigdahl B, Krebs FC. Combinatorial approaches to the prevention and treatment of HIV-1 infection. *Antimicrob Agents Chemother* 2011; **55(5)**:1831-1842.

41. Chonco L, Pion M, Vacas E, Rasines B, Maly M, Serramia MJ, *et al.* Carbosilane dendrimer nanotechnology outlines of the broad HIV blocker profile. *J Control Release* 2012; **161(3)**:949-958.

42. He C, Hu Y, Yin L, Tang C, Yin C. Effects of particle size and surface charge on cellular uptake and biodistribution of polymeric nanoparticles. *Biomaterials* 2010; **31(13)**:3657-3666.

43. Jiang W, Kim BY, Rutka JT, Chan WC. Nanoparticle-mediated cellular response is size-dependent. *Nat Nanotechnol* 2008; **3(3)**:145-150.

44. Gao X, Wu B, Zhang Q, Chen J, Zhu J, Zhang W, *et al.* Brain delivery of vasoactive intestinal peptide enhanced with the nanoparticles conjugated with wheat germ agglutinin following intranasal administration. *J Control Release*

2007; **121(3)**:156-167.

45. Vercauteren D, Vandenbroucke RE, Jones AT, Rejman J, Demeester J, De Smedt SC, *et al.* The use of inhibitors to study endocytic pathways of gene carriers: optimization and pitfalls. *Mol Ther* 2010; **18(3)**:561-569.

46. Riddell FG, Arumugam S, Cox BG. The monensin-mediated transport of Na+ and K+ through phospholipid bilayers studied by 23Na- and 39K-NMR. *Biochim Biophys Acta* 1988; **944(2)**:279-284.

47. Zeng N, Hu Q, Liu Z, Gao X, Hu R, Song Q, *et al.* Preparation and characterization of paclitaxel-loaded DSPE-PEG-liquid crystalline nanoparticles (LCNPs) for improved bioavailability. *Int J Pharm* 2012; **424(1-2)**:58-66.

Figure Legend

Fig. 1. Schematic illustration. (a) Schematic of T1144-NP-14f assembly. NPs were composed of a biodegradable PLA core for drug encapsulation and PEG chain for particle stability. (b) Schematic diagram of HIV-1 and nanoparticle (T1144-NP-14f) trafficking and the putative mechanism of action of T1144-NP-14f to inhibit viral-cell membrane fusion.

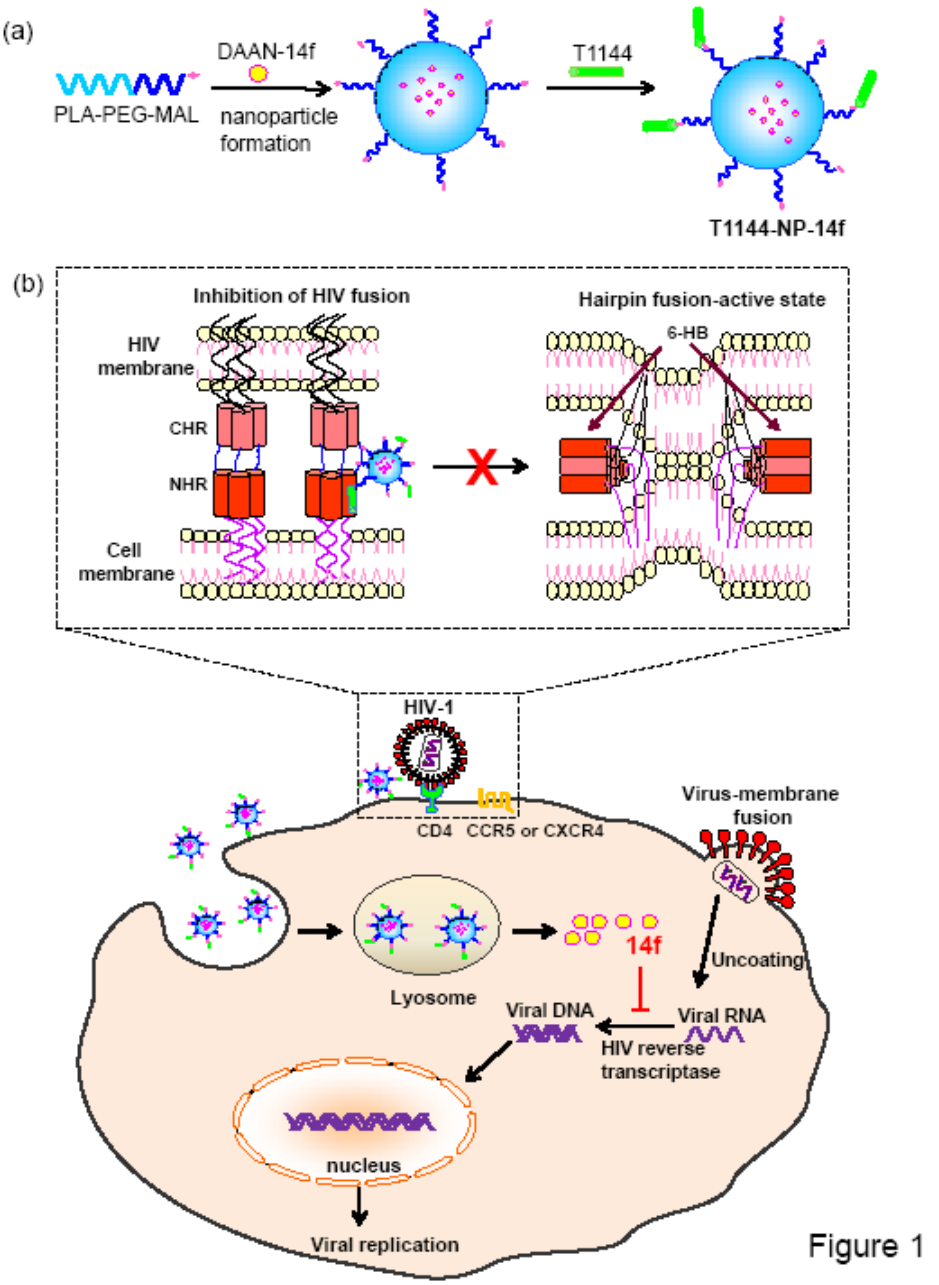

Figure 1

Fig. 2. Characterization of T1144-NP-14f. Size distribution of blank NP (a), NP-14f (b), and T1144-NP-14f (c) was measured by dynamic light scattering (DLS), respectively. Transmission electron microscopy (TEM) images of blank NP (d), NP-14f (e), and T1144-NP-14f (f). Bar: 100 nm. CLSM images of Rhodamine-T1144-NP-coumarin-6 assembly (g). NPs were loaded with coumarin-6, and T1144 was conjugated with Rhodamine for imaging (Rhodamine-T1144-NP-coumarin-6). Scale bar is 50 μm.

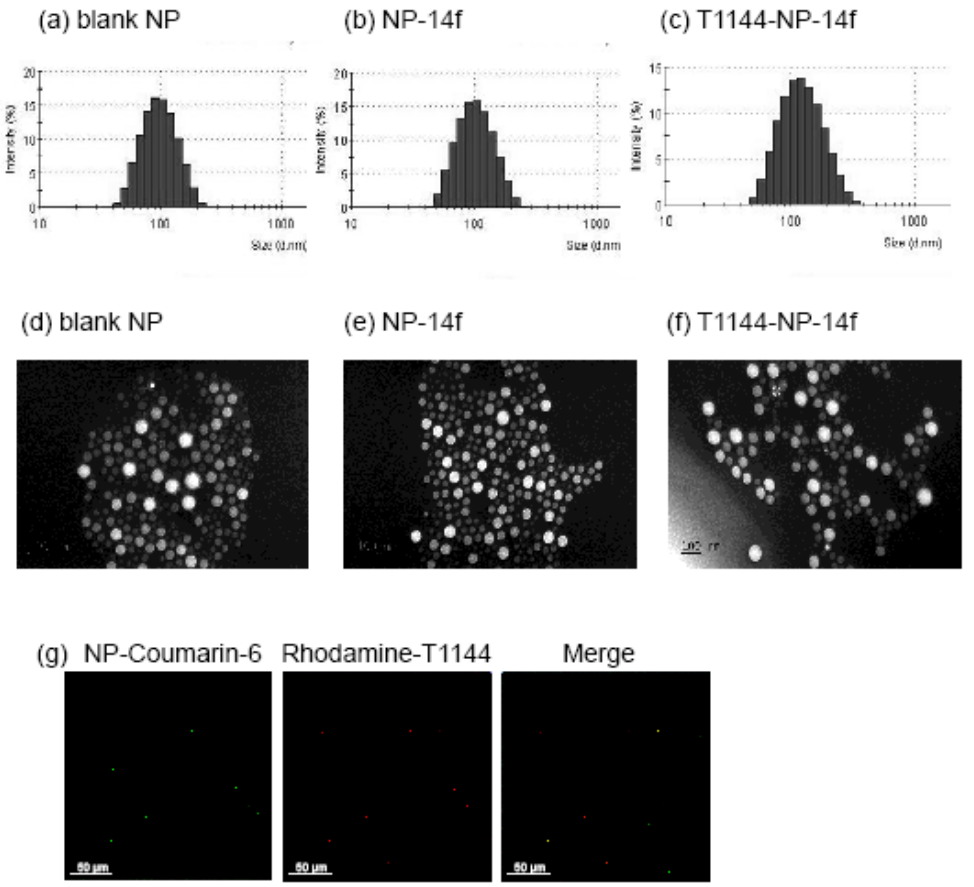

Figure 2

Fig. 3. Quantitative measurement of *in vitro* uptake of T1144-NP-coumarin-6, NP-coumarin-6, and coumarin-6 solution in MT-2 cells and M7 cells. Cellular uptake of T1144-NP-coumarin-6, NP-coumarin-6, and coumarin-6 solution was detected at different temperatures (4 ºC and 37 ºC) after incubation for 2 h at coumarin-6 concentrations ranging from 25 to 600 ng/ml in MT-2 cells (a), and M7 cells (b). The uptake of T1144-NP-coumarin-6 and NP-coumarin-6 were much higher than coumarin-6 solution at both 4 ºC and 37 ºC. Cellular uptake of T1144-NP-coumarin-6, NP-coumarin-6, and coumarin-6 solution in MT-2 cells (c), and M7 cells (d) after incubation for 0.5 to 8 h at the coumarin-6 concentration of 200 ng/ml. T1144-NP-Coumarin-6 exhibited significantly higher fluorescence intensity than that of coumarin-6 solution at every experimental time point. Each sample was tested in triplicate, and the experiment was repeated twice with similar results. The data are presented as mean ± SD (bars) from a representative experiment. $*P < 0.05$, $**P < 0.01$, $***P < 0.001$.

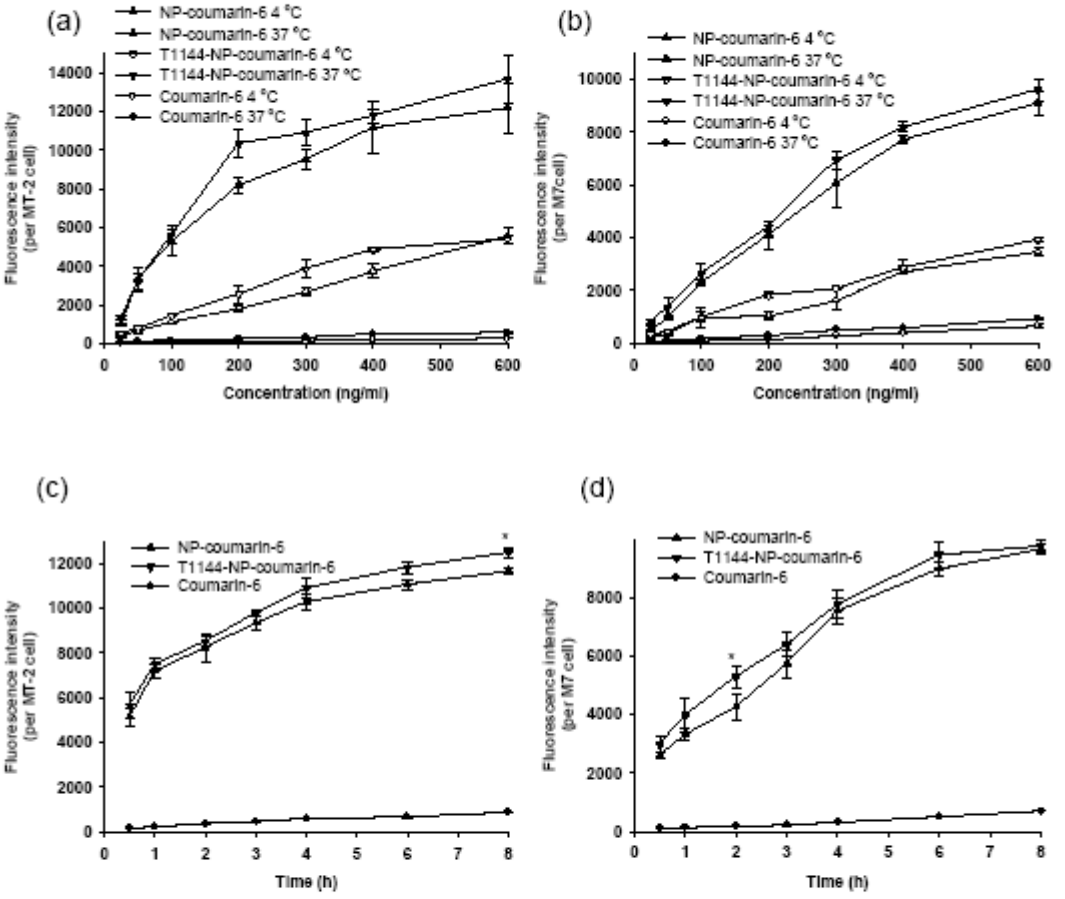

Figure 3

Fig. 4. Inhibitory activity of T1144-NP-14f. (a) The inhibitory activity of T1144-NP-14f against 6-HB formation between N36 and C36 was detected by ELISA. (b) Inhibition of HIV-1 Env-mediated cell-cell fusion. (c) The inhibitory activity of T1144-NP-14f against infection by HIV-1 IIIB (subtype B, X4) in MT-2 cells. (d) The inhibitory activity of T1144-NP-14f against infection by HIV-1 Bal (subtype B, R5) in M7 cells. Each sample was tested in triplicate; the data are presented as mean ± SD.

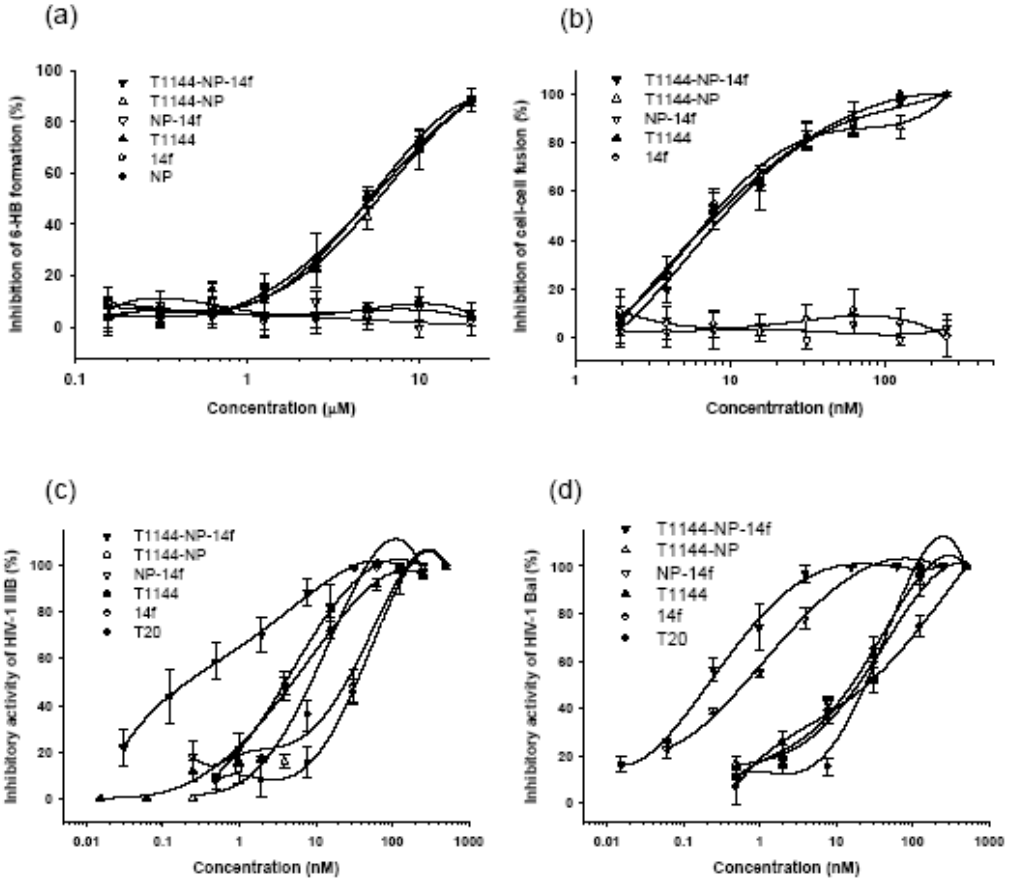

Figure 4

Fig. 5. *In vitro* release and *in vivo* pharmacokinetic studies of 14f solution, NP-14f, and T1144-NP-14f. (a) *In vitro* cumulative release of 14f from 14f solution, NP-14f, and T1144-NP-14f in PBS (pH 7.4) with 0.1% Tween-80 at 37 ^{o}C. (b) Plasma 14f concentration-time curves after i.v. administration of 14f, NP-14f, and T1144-NP-14f to SD rats at a dose of 5 mg/kg through the tail vein. At predetermined time points, blood samples were collected and determined. Each sample was tested in triplicate.

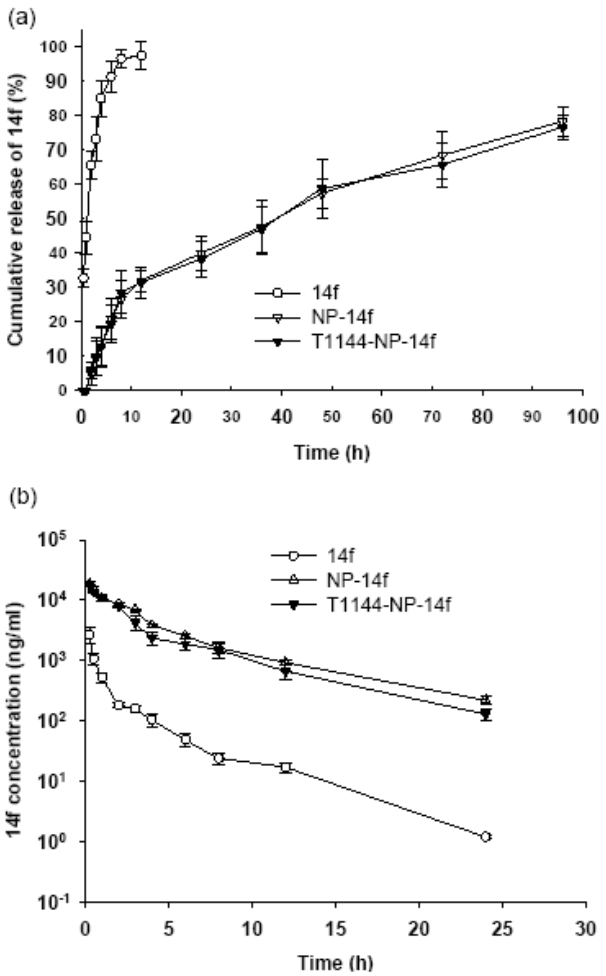

Figure 5